# Investigation of Molten Liquids Flow in the Blast Furnace Lower Zone: Numerical Modelling of Molten Slag Through Channels in a Packed Bed

X.F. DONG, A. JAYASEKARA, D. SERT, R. FERREIRA, P. GARDIN, B.J. MONAGHAN, S.J. CHEW, D. PINSON, and P. ZULLI

Slag flow behaviour is critically important in the lower zone of the ironmaking blast furnace, and is closely related to the selection of charged raw materials, coke bed permeability, process stability and hot metal quality. To better understand the effect of slag properties on flow behaviour in the coke bed, a numerical approach was applied to characterize the slag flow through funnel analogues. These analogues were used to represent molten slag flow through the inter-particle voids of a coke packed bed. A critical funnel neck size, through which no slag flowed was experimentally established and confirmed by numerical modelling. The influence of slag wettability on the occurrence of blockage was also determined via numerical modelling. An increase in either contact angle or surface tension can make the occurrence of blockage easier. For a constant neck size, the relationship between surface tension and contact angle is non-linear. The status of the remaining slag in the funnel corresponding to different slag wettabilities was differentiated in terms of the blockage in the upper part and hanging in the lower part of the funnel. Modelling was also undertaken of slag flow through the inter-particle void between spherical particles to evaluate empirical correlations for predicting the remaining slag in the packed bed. These results show that the numerical approach is very useful in providing some level of guidance to help understand and predict the slag flow behaviour in the blast furnace ironmaking process.

## I. INTRODUCTION

MOLTEN slag is a critical material in blast furnace (BF) ironmaking, being initially generated in the softening-melting zone and flowing through the lower part of the BF before being discharged from the hearth. It influences hot metal quality, process stability and hence, overall operating cost. Slag generation is closely related to the quality of the charged materials used in the BF. The increasing use of poorer quality materials and the requirement for decreasing the amount of carbonaceous materials used in ironmaking are affecting slag volumes and compositions.[1] Understanding these changes and their effects on slag properties are key research drivers in BF ironmaking. Specifically, an improved knowledge of the effect of slag properties on the permeability in the lower part of the BF is required if current BF productivity levels are to be maintained or even improved.

The flow of reducing gas and liquids (iron and slag) in the lower zone of the BF is often characterized as flow through a coke packed bed.[2] A change in slag properties can result in the local accumulation of liquid in the coke bed, changing the bed permeability and gas distribution. Beyond a certain limit, such conditions can lead to liquid flooding and poor BF stability. In this regard, the liquid flow behaviour in the BF has been investigated under different conditions, including one- and two-dimensional experimental configurations. Early studies focused on generation of holdup correlations and understanding the flooding phenomena by using one-dimensional experimental facilities[3–9] and identification of flow regimes and investigation of the effect of bed structure in two-dimensional apparatus[10–13] under room temperature (RT) conditions.

X.F. DONG, A. JAYASEKARA, and P. ZULLI are with the School of Mechanical, Materials, Mechatronic and Biomedical Engineering, University of Wollongong, Wollongong, NSW 2522, Australia and also with the ARC Research Hub for Australian Steel Manufacturing, University of Wollongong, Wollongong, NSW 2522, Australia. Contact e-mail: xuefeng.dong@uow.edu.au. D. SERT, R. FERREIRA, and P. GARDIN are with the ArcelorMittal Maizieres Research SA, 57283 Maizéres-lés-Metz, France. B. J. MONAGHAN is with the School of Mechanical, Materials, Mechatronic and Biomedical Engineering, University of Wollongong. S.J. CHEW and D. PINSON are with the Coke & Ironmaking Technology, BlueScope Ltd, Wollongong, NSW 2522, Australia.

Recently, the liquid flow behaviour and holdup distribution were studied under more realistic,[14–21] high-temperature (HT) conditions. These high-temperature experiments were carried out based on either packed beds[14,15,17,20] or funnel analogue conditions.[18,22] Liquid flow through a funnel was used to simulate either the slag flow through a pore between coke particles[18] or the dripping behaviour of slag from the reduced metallic iron or unreduced ore particles.[22] Experimental results show that residual slag in the coke packed bed or channel in the funnel is significantly controlled by slag wettability.[14] It was confirmed that reaction between slag and coke mineral matter causes the slag to change from non-wetting to wetting in the coke bed, particularly for cokes with higher mineral contents.[15,18,21] Slag and iron appears to flow concurrently in a funicular type of flow, i.e. the iron flows through the core of the void, and the slag flows between the coke and iron.[15] It was also observed that the residual slag exists in the funnel in different forms such as slag blockage within the funnel[18] or held up below the funnel.[22]

To quantitatively describe the liquid flow, numerical models have been proposed to describe the gas and liquid flows in the BF within the framework of continuum and other approaches, including potential flow,[23,24] probability,[25] probability-continuous,[26] tube network dynamic,[27] force balance[28–30] and Volume of Fluid (VOF)[16,31] models. Most models are mainly used in simulation at a large scale. Theoretically, it remains difficult to simulate the division, collection, coalescence and deformation of liquid droplets using the continuum approach with an assumption of an interpenetrating continuous media. In particular, for high-temperature conditions, the variation of phase properties together with the interactions between phases in relation to changing interfaces, make simulation more complex. Recent application of the VOF model in modelling slag-iron flow[16,31] at a particle scale demonstrated a promising capability in capturing the moving interface between phases and the change of interface (between iron and slag) that enhanced the passage of higher carbon iron through the coke slit.

At a particle scale, a discrete approach presents a capability to model the coalescence of droplets.[32–39] Although the study of the movement of liquid droplets is still at an early stage, the detailed micro-dynamic information provided by discrete techniques has assisted in understanding the influence of key factors on liquid flow behaviour.

However, there are limited numerical studies of wettability in relation to slag properties. In this study, a numerical investigation was carried out to assess the influence of wettability on the flow of molten liquids through the channel of a funnel analogue, representing the flow of molten liquids through the inter-particle voids of a coke packed bed. A computational fluid dynamic (CFD) model was developed and validated through different conditions to provide a deeper understanding of molten slag flow behaviour in the funnel. Specifically, the model was used to assess the effect of changing slag properties such as wetting angle and surface tension on critical slag flow conditions, and to further investigate the slag flow behaviour between the spherical particles.

## II. MATHEMATICAL MODEL

The Volume of Fluid (VOF) method[40] was applied to describe immiscible multiphase flows with distinct interfaces in a funnel geometry using the fluid volume fraction in a computational cell to track the interface between the phases. To locate the interface in each cell of the free surface, a piecewise linear interface construction (PLIC) method[41] was applied so that the interface can be approximately represented by an oriented line segment. The general governing equations for mass and momentum transfer are given in Table I, Eqs. (1) through (4). Computations were carried out using the ANSYS-Fluent (v19.1) platform.

In the continuity equation, also called the volume fraction equation, $\varepsilon_i$ is the volume fraction of phase i, $u$ is velocity and $t$ is time. Solution of the continuity equation is used to track the interface between the phases. In the momentum equation, the surface tension force, $F$, which is a function of surface tension between two phases $i$ and $j$, $\sigma_{ij}$, is used to account for the interaction between the phases and between the phases and the wall. A single momentum equation is solved throughout the domain, and the resulting velocity field is shared among the phases. The physical properties of the mixture such as density, $\rho$, and viscosity, $\mu$, are volume-fraction-averaged, i.e.

$$\rho = \sum \varepsilon_i \rho_i \qquad [5]$$

$$\mu = \sum \varepsilon_i \mu_i \qquad [6]$$

$$\sum \varepsilon_i = 1 \qquad [7]$$

$\kappa_i$ is the curvature of the interface, expressed as

$$\kappa_i = \nabla \cdot (\nabla \varepsilon_i / |\nabla \varepsilon_i|) \qquad [8]$$

Table I.  Governing Equations

| Equations | Descriptions | |
|---|---|---|
| Continuity Equation | $\frac{\partial \varepsilon_i}{\partial t} + \nabla \cdot (\varepsilon_i \boldsymbol{u}) = 0$ | (1) |
| Momentum Equation | $\frac{\partial}{\partial t}(\rho \boldsymbol{u}) + \nabla \cdot (\rho \boldsymbol{uu}) = -\nabla p + \nabla \cdot \boldsymbol{\tau} + \rho \boldsymbol{g} + \boldsymbol{F}$ | (2) |
| | $\boldsymbol{\tau} = \mu \left[ \nabla \boldsymbol{u} + (\nabla \boldsymbol{u})^T \right]$ | (3) |
| | $\boldsymbol{F} = 2\rho \kappa_i \sigma_{ij} \nabla \varepsilon_i / (\rho_i + \rho_j)$ in case of two phases | (4) |

The following assumptions were imposed for the mathematical modelling of liquid flow in the funnel geometry:

- Incompressible multiphase flow
- No mass transfer between phases
- No variations in the surface tension coefficient
- Phases are immiscible with a clearly defined interface
- No mass generation
- The system is in a thermal equilibrium
- Phases share the same velocity field
- Laminar flow

The initial and boundary conditions were

### A. *Initial Condition*

At the beginning of each simulation, the liquid region was patched at the corresponding position in the computational domain. The patch was initialized with a volume fraction set to unity for the specified liquid phase and a zero velocity. For validation cases, the initial liquid region has the same liquid volume as that used in the setup of experiments.

### B. *Wall*

A no-slip boundary condition was imposed for the liquid velocities at the wall. The effects of wall adhesion at phase interfaces in contact with the wall boundary can be estimated considering the contact angle of each phase at the wall $\theta_{iw}$ in the evaluation of the interfacial curvature near the wall.[42] This is described by

$$\kappa_i = \nabla \cdot (\hat{n}_{iw} \cos \theta_{iw} + \hat{t}_{iw} \sin \theta_{iw}) \qquad [9]$$

where $\hat{n}_{iw}$ and $\hat{t}_{iw}$ are the unit vector normal and tangential to the wall and $\hat{n}_i$ is the unit normal vector at the interface, expressed by

$$\hat{n}_i = \nabla \varepsilon_i / |\nabla \varepsilon_i| \qquad [10]$$

### C. *Outlet and Opening*

A pressure outlet boundary condition was set for the outlet at the bottom and the opening at the top of funnel.

The following methodologies were adopted in the simulation:

- Explicit formulation was used to calculate the volume fraction
- Body force was implicitly treated

- A second order upwind scheme[43] was used for the discretization of convective terms
- The temporal derivatives were discretized using a first order implicit method[43]
- The geometric reconstruction scheme[43] was used for the calculation of face fluxes
- The gradient used to discretize the convection and diffusion terms was Green-Gauss node based[44]
- The velocity-pressure coupling was solved based on the SIMPLE algorithm[45]
- Fully structured grids were generated for an accurate calculation of surface tension.

Numerical simulations were carried out for different liquids used in both low and high-temperature experimental conditions. The properties of liquids used in the subsequent sections are given in Table II. Water, Slag A and Slag B were used in the model validations corresponding to the liquids utilized in experiments. Slag C was used in the model application to investigate the effect of wettability on the liquid flow in Section IV. The slag properties including surface tension, viscosity and density were calculated via NPL[46] and Riboud[47] models. Water properties were based on published literature.[48]

## III. MODEL VALIDATION BASED ON RT AND HT FUNNEL EXPERIMENTS

Numerical modelling was carried out for different funnel experimental conditions, *i.e.* water flow in the RT simulations and slag flow in the HT simulations. The RT experiments were conducted to visualize the liquid flow behaviour in the funnel and provide experimental data for validating the numerical model. The HT experimental conditions were based on the literature data with an identified amount of retained slag in the funnel.[18,22]

### A. *Modelling of Water Flow in Room Temperature Funnel Experimental Conditions*

A schematic of the RT experimental apparatus is shown in Figure 1. A 50 mL burette, with a needle of ~ 0.57 mm diameter (ID) attached to the outlet, was used as a reservoir to deliver liquid to a funnel. The funnel was made from plexiglass. Three funnels with different neck diameters of 1, 2 and 3 mm were used. The geometry of a funnel with a neck diameter of 1 mm is given in Figure 1(b) as an example. The angle of the inclined surface in the upper part of each funnel was 60

Table II. Properties of Liquids Used in the Simulation

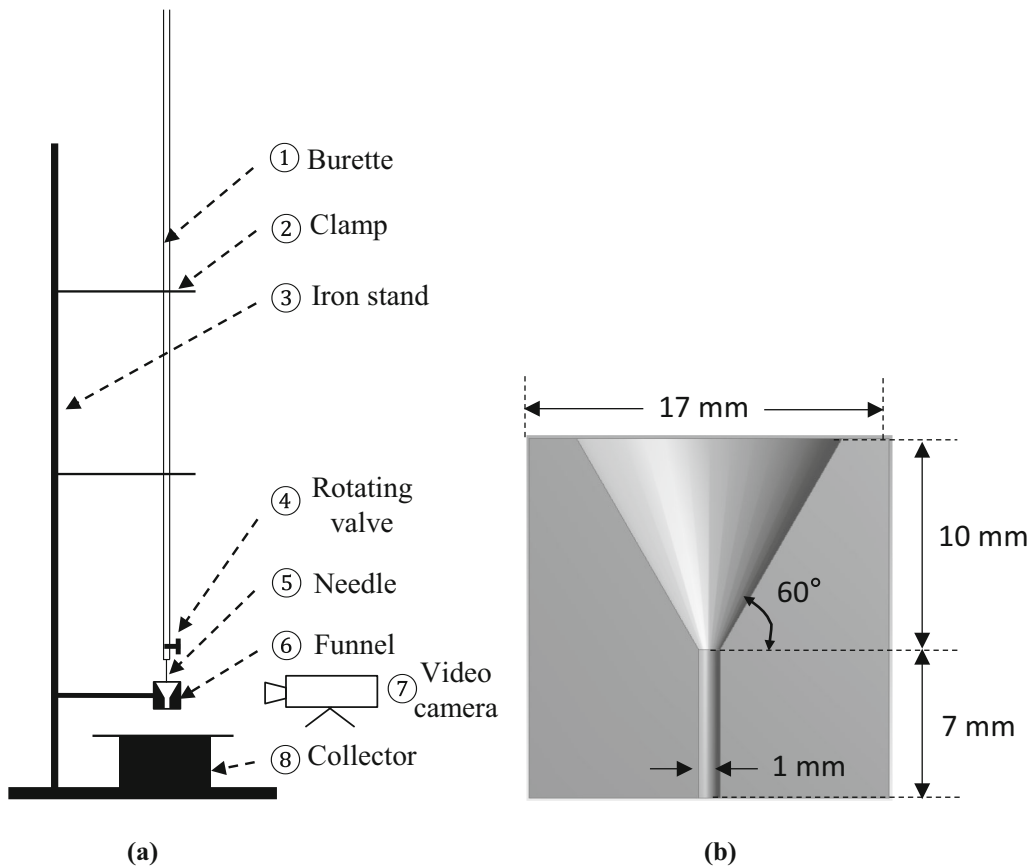| Liquid | Composition in Mass Pct | | | | | Viscosity, $\mu$, Pa s | Surface Tension, $\sigma$, N m$^{-1}$ | Density, $\rho$, kg m$^{-3}$ | T, °C |
| | CaO | SiO$_2$ | Al$_2$O$_3$ | MgO | FeO | | | | |
|---|---|---|---|---|---|---|---|---|---|
| Slag A | 44.0 | 34.5 | 12.2 | 8.8 | — | 0.178 | 0.504 | 2686 | 1500 |
| Slag B | 20.2 | 22.1 | 24.7 | — | 33.0 | 0.856 | 0.558 | 3188 | 1400 |
| Slag C | 40.7 | 37.4 | 12.5 | 8.8 | — | 0.264 | 0.493 | 2675 | 1500 |
| Water | — | — | — | — | — | 0.001 | 0.0732 | 998 | 20 |

Fig. 1—(*a*) Schematic of the room temperature experimental apparatus (① burette; ② clamp; ③ iron stand; ④ rotating valve; ⑤ needle; ⑥ funnel; ⑦ video camera; ⑧ collector); (*b*) geometry of the funnel with a neck diameter of 1 mm.

deg, which is based on the high-temperature experimental setup in the literature.[18] The contact angle between water and plexiglass is required to solve Eq. [9]. This was measured to be 71.8 deg determined using an optical tensiometer (USA Kino SL200KS).

Prior to carrying out the experiment, the internal surface of funnel was cleaned and dried, *i.e.* the funnel was firstly rinsed with water, then dewatered by manual spinning and finally left in a clean container for ~ 2 hours natural drying. The horizontal level of funnel was established using a spirit level.

In the funnel with a neck diameter of 1 mm, the water can accumulate without any "stopper" at the outlet of the funnel. For larger neck diameters, water accumulation in the funnel required a "stopper". Once water accumulated to a level of 7 to 9 mm above the neck, the "stopper" was removed and the flow behaviour was recorded using a Sony FDR-AXP55 8.3 MP video camera.

Figure 2 shows the initial ((a) through (c)) and corresponding final conditions ((d) through (f)) for three different funnel neck diameters (1, 2 and 3 mm), respectively. These results show that the amount of liquid remaining in the funnel is very sensitive to the neck size assuming that the other conditions remain constant. Note that the dash lines in Figure 2 approximately delineate the boundary of water in the funnel.

Numerical modelling was carried out based on the room temperature experiments using water. Three funnels with diameters 1, 2 and 3 mm were used in the simulation, respectively. Figure 3 shows a typical computational domain which corresponds to a funnel with a diameter 3 mm. For computational efficiency, only one quarter of the flow domain was taken into account, but the simulation was still conducted in three-dimensions. Side elevations of the computational domain in 3D view were treated as symmetric surfaces, highlighted in Figure 3(a). Figure 3(b) shows the fully connected multi-block structured mesh distribution for each side elevation. The 3D domain was composed of ~ 0.25 M elements with a sufficiently fine mesh to capture the liquid interface curvature, and interaction between the liquid and wall surface. The water properties used in the simulation are given in Table II.

Simulations were carried out under different funnel conditions. The measured heights of water in the funnel were used as the initial condition in the simulations (Figures 4(a), (c) and (e)), together with the corresponding final steady-state results (Figures 4(b), (d) and (f)). Similar to the experimental results, simulation results show that the flow of water is prevented (blocked) at the neck of a channel with a diameter of 1 mm. The water can flow through the other funnels with larger neck diameters. The height of remaining water in the channel decreases with increasing neck diameter. The water
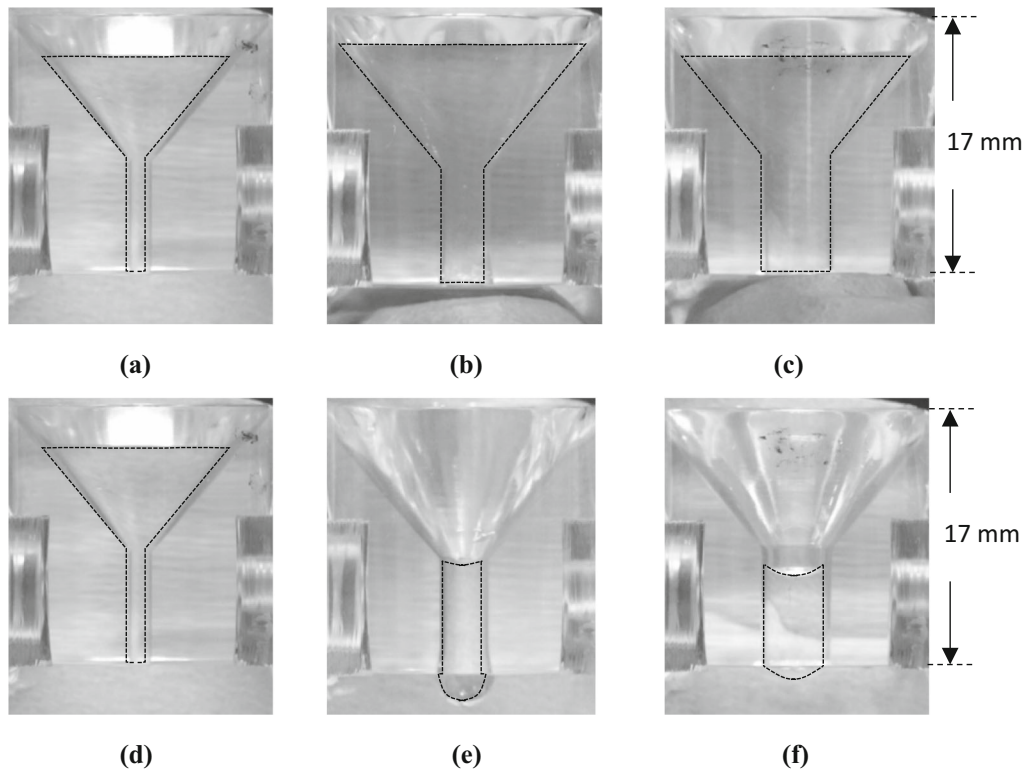
Fig. 2—Initial liquid conditions (*a*) through (*c*) and corresponding final conditions (*d*) through (*f*) for room temperature funnel experiments with neck diameters of: (a, d) 1 mm, (b, e) 2 mm, (c, f) 3 mm.
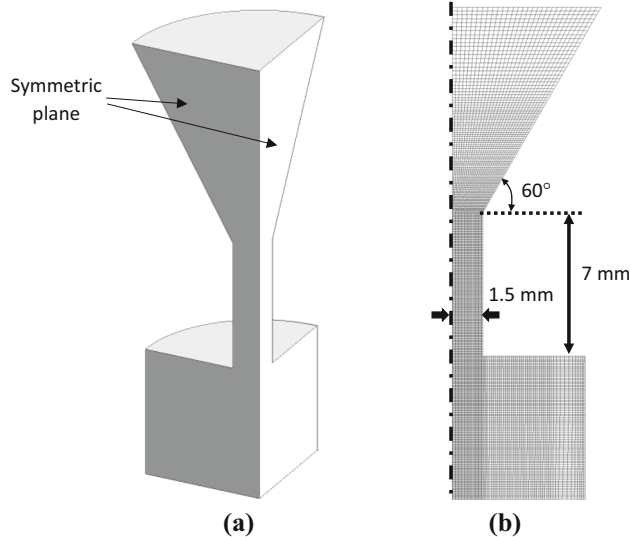


Fig. 3—(*a*) 3D view of the reduced computational domain, and (*b*) mesh distribution on the side face for a funnel with a neck diameter of 3 mm. Note: the funnel radii are reported.

heights in the funnel channel with neck diameters of 2 and 3 mm are ~ 8.3 and ~ 6.1 mm (experimental), 8.4 and 3.1 mm (simulated), respectively. Calculated less water volume remaining in the channel (Figure 4(f)) can be a key reason for a less curved lower surface compared to experimental result (Figure 2(f)). Note that the

plexiglass funnels used in the experiment were machined and then polished, rather than cast via moulds. Imperfections on the internal funnel surface and transition region may cause the variation of adhesive force between water and funnel surface. This variation can affect the water flow behaviour in the funnel and the curvature of water-air interface at the final stage. Therefore, the comparison between experimental and simulated results is qualitative.

### B. Modelling of Slag Flow in HT Funnel Experimental Conditions

#### 1. Blockage phenomenon for a non-wetting slag flow through a funnel

In a previous study,[18] it was found that there is a minimum channel diameter (neck diameter) required to allow the free flow of slag through the funnel before any significant interfacial reactions occur.

To further test the application of the numerical model for HT conditions, a simulation was set up based on previous experimental conditions,[18] as shown in Figure 5(a). The funnel material was a coke analogue, made from carbonaceous materials and used for the study of metallurgical cokes.[18] In the funnel, the channel length was 7 mm and different channel diameters were applied (1.5 to 5.0 mm). The angle of the inclined surface in the upper part of funnel is 60 deg. During the HT experiment, a cylinder shaped slag pellet with mass of 1.42 g and diameter of 10 mm, was placed in the upper part of funnel. The funnel and slag were heated to 1500
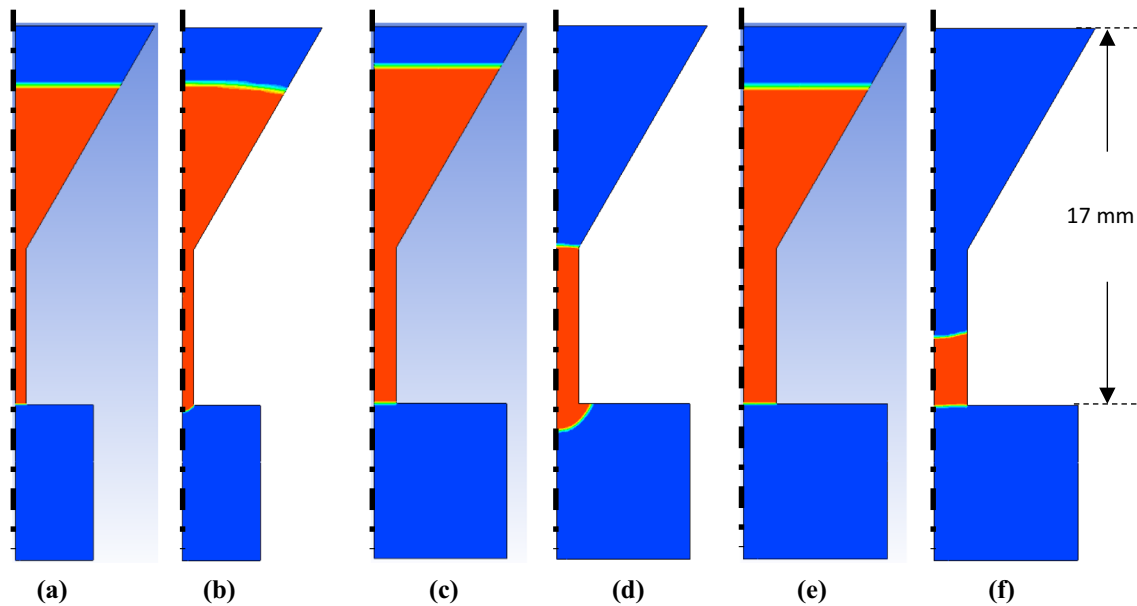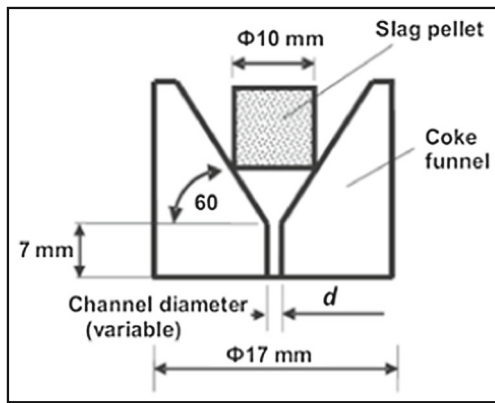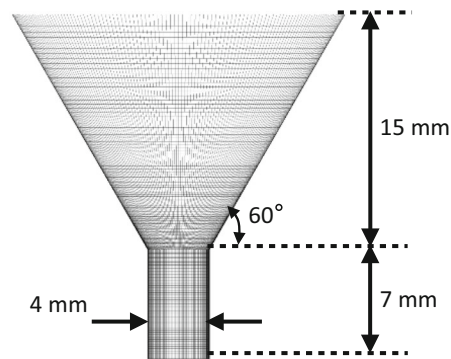
Fig. 4—Initial conditions and final steady-state results for water in the funnel with different neck diameters: 1 mm (*a*) through (*b*), 2 mm (*c*) through (*d*) and 3 mm (*e*) through (*f*). Note that the initial liquid heights in the three funnels are 14.35, 15.13 and 14.38 mm, respectively.



Fig. 5—(*a*) High-temperature experimental setup [18]; (*b*) front view of mesh and dimensions of computational domain. Reprinted from Ref. 18, with permission.

°C in an inert atmosphere and then held at this temperature for 30 minutes before cooling to the room temperature. After cooling, the sample (funnel and slag) was removed for characterization.

A corresponding full three-dimensional computational domain was set up and is shown in Figure 5(b). A neck diameter of 4 mm was used, which corresponded to a "blocked" flow condition for a particular slag composition (Slag A) given in Table II. The internal surface of the funnel was assumed to be smooth. A fully structured hexahedral mesh was generated for the funnel so as to improve the solution accuracy and reduce the number of elements in the simulation.

Figures 6(a) through (b) show the initial conditions and typical simulation results for blocked flow at 0.2 second. The initial height of the liquid in the funnel was 8.124 mm above the top of the channel. A contact angle of 160 deg between Slag A and the funnel material was assumed with reference to measurements in the literature.[14] In the simulation results, both upper and lower surfaces of the liquid near the wall show a typical non-wetting characteristic. The surface curvature is decided by a balance between gravity and adhesive forces between slag and solid wall. The result shows an extruded central part of the slag droplet, causing the lower surface of slag to significantly deform, such that
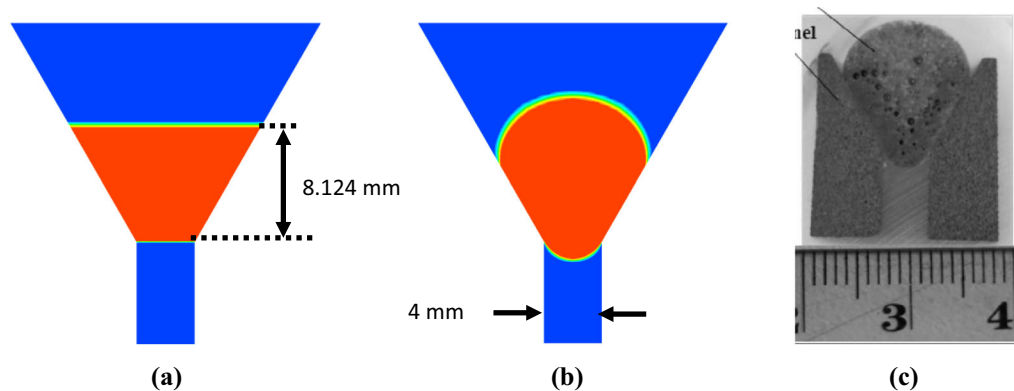
Fig. 6—Simulation results at (*a*) 0 s and (*b*) 0.2 s; experimental results for slag blockage in the funnel: (*c*) a section of a funnel.[18] Reprinted from Ref 18, with permission.
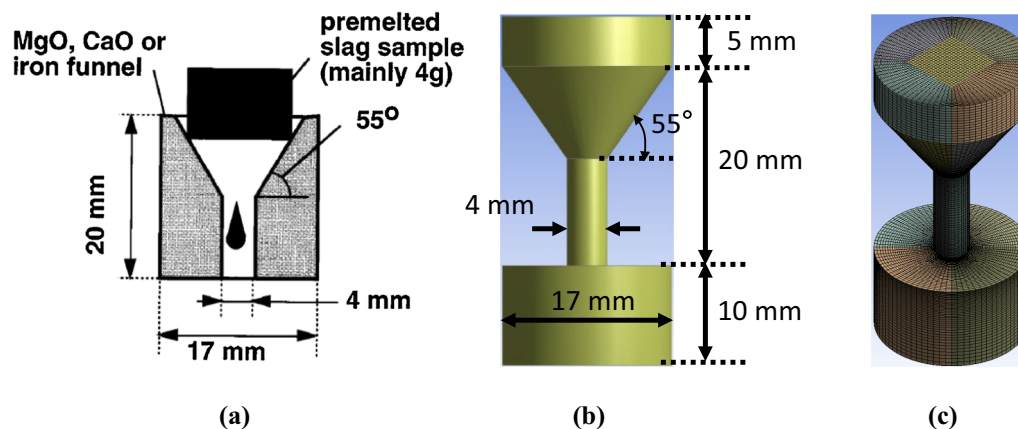


Fig. 7—(*a*) Experimental funnel setup[22]; (*b*) dimensions of computational domain; (*c*) computational mesh.

the capillary force between slag and wall increases until this is balanced against the weight of the droplet (gravity). The capillary force is sufficiently strong to stop the flow of liquid at the entrance of the channel, which is confirmed by slag not flowing through the coke channel (Figure 6(c)). The comparison between experimental results from previous research[18] (see Figure 6(c)) and the corresponding numerical simulation result (see Figure 6(b)) is good. The heights of remained slag in the experimental and simulation results are ~ 14.0 and 11.6 mm, respectively.

### 2. Hanging phenomena for a wetting slag flow through a funnel

Compared with the blockage phenomena, Hino *et al.*[22] used funnel experiments to identify strong wetting phenomena for a FeO-CaO-SiO$_2$-Al$_2$O$_3$ slag system (Slag B, Table II). In their experiments, the funnel was made from either iron, CaO or MgO. The synthetic Fe$_t$O-containing slag flowed through the funnel to simulate the dripping behaviour of the slag from reduced metallic iron or unreduced ore particles. The angle of the inclined surface in the upper part of this funnel was 55 deg. The channel neck diameter was 4 mm. During the experiment, a slag tablet with an initial mass of 4 g was first put on the funnel and then heated under inert atmosphere. The weight change of the sample was continuously monitored by a thermo-balance. The sample was finally cooled to room temperature for measurement.

Hino *et al.*[22] observed that the slag flowed through the funnel and then wetted, or attached to, the lower surface of the funnel. The shape of the liquid slag hanging below the funnel was found to be predominantly related to the extent of slag wettability of the funnel materials used. Their data provided further opportunity to validate the numerical model described previously. As shown in Figure 7(b), a computational domain was set up to reproduce their experimental setup.[22] The space below the funnel was also considered in the simulation to enable the possible hanging phenomena to be calculated. A structured mesh was generated as shown in Figure 7(c).

The slag properties used in the simulation are given in Table II. Note that the contact angle was not provided by Hino *et al.*[22] A value of 60 deg was assumed. The choice of this value was based on the wetting nature of high FeO-containing slag shown in the Hino *et al.*[22] study and that reported elsewhere.[49]

Figures 8(a) through (c) show the calculated liquid distributions at times of $t = 0.0$, 4.0, and 8.0 seconds, respectively. Simulation results show that the slag accumulates and spreads at the lower surface of the funnel. After a droplet falls from the funnel, the slag finally forms a dome shape below the funnel. Qualitatively, these results are comparable with Hino et al.'s experimental observations.[22] These results present a large spreading diameter, with the dome shape maintained at the final experimental stage. The height/width of domes in the experimental observations and simulation results are ~ 7.8/15.2 and 4.7/11.5 mm, respectively. In this wetting condition case, the major driving force for spreading is the capillary force along the lower surface of the funnel.

In summary, the non-wetting and wetting behaviours of slag described in this section identify two possible phenomena for slag holdup within the BF coke bed: (a) for non-wetting conditions, the possibility of the interstitial space above particles retaining or being blocked by slag; and (b) for wetting conditions, the possibility of the interstitial space below particles being blocked by slag adherence to the particles. These phenomena are differentiated by the slag wettability.
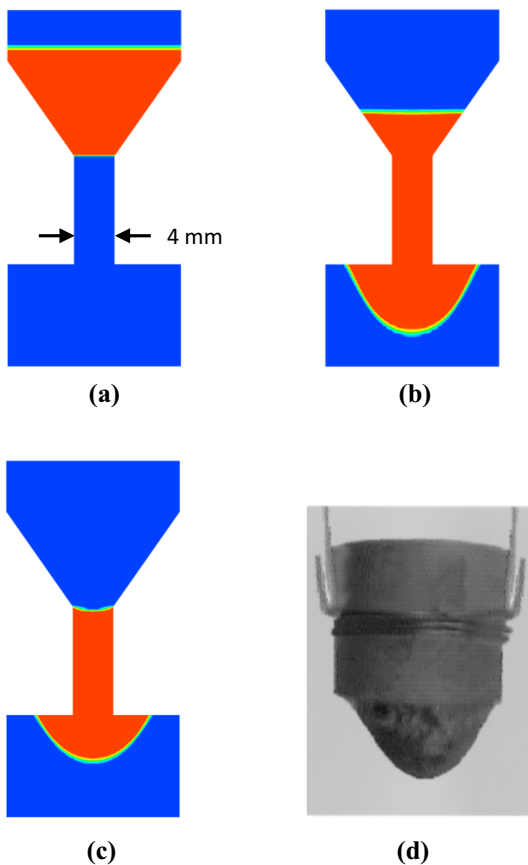


**(a)**  **(b)**

**(c)**  **(d)**

Fig. 8—Simulation results for Slag B (33 wt pct FeO) at different times: (a) 0, (b) 4.0 and (c) 8.0 s; experimental results: (c) a view of the iron funnel after the experiment.[22] Note that the initial height of slag in the funnel is 10.81 mm.

## IV. MODEL APPLICATION

### A. Critical Conditions for Blockage of Non-wetting Slag Above Channels

A series of simulations with varying surface tension and contact angles were carried out for the non-wetting liquid, Slag C, in order to determine its flow behaviour (blocked or unblocked flow) through funnel channels with different neck diameters, viz. 4.4 or 5 mm. As surface tension refers to the cohesive force within the slag and the contact angle reflects the interfacial tension between slag and funnel materials, it is expected that the influence of wettability on slag flow can be well represented. Excluding the neck diameters, the funnel profile is the same as Figure 5(b). The initial height of the liquid in the funnel was 10 mm. The other properties of Slag C used in the simulation are listed in Table II. The results, which are summarized in Figure 9, highlight the relationship between liquid properties in terms of surface tension and contact angle and the blockage of liquid slag. With a large contact angle, liquid slag with relatively low surface tension will lead to a blocked flow condition. As the contact angle decreases, liquid slag flow into the funnel channel becomes easier. It should be noted that the exact transition between blocked and unblocked flow given in Figure 9 is closely related to the initial height of the liquid. It is expected that for a higher initial liquid height, the unblocked flow region will expand. However, the relative relationship between contact angle and surface tension should maintain a similar trend.

Corresponding to each channel diameter, in terms of the occurrence of blockage, the relationship between contact angle and surface tension is non-linear. At high contact angles (> 160 deg), the surface tension leading to blockage is almost constant, but for lower contact angles (140 to 160 deg), the surface tension that is required to cause blockage is much higher. As the channel diameter increases from 4.4 to 5 mm, for the same contact angle, an increase of 20 to 30 pct in surface tension can block flow. Note that dot and triangle symbols in Figure 9 refer to the calculated results using funnels with a neck diameter of 4.4 and 5 mm, respectively. Solid and hollow symbols correspond to occurrences of unblocked and blocked flow,



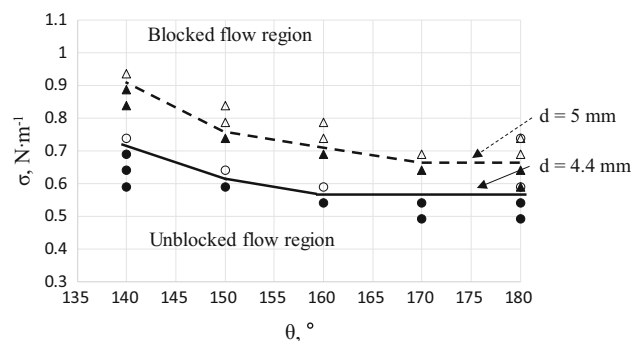Fig. 9—Relationship between liquid properties, contact angle and surface tension, and the blockage of liquid slag in the funnel. Note that d refers to the diameter of the channel in the funnel.

respectively. Considering that the interstitial space between particles, which the channel represents, is a function of packed particle size, Figure 9 indirectly shows the effect of coke particle size on liquid slag flow. Larger particle sizes are associated with less blockage, and therefore smoother slag flow through the packed bed.

In a BF, as the slag forms within the cohesive zone and drips through the coke bed, the wettability of slag with the packed coke particles may change significantly from wetting to non-wetting conditions due to the variation of slag composition, temperature and packing properties. In particular, small coke particles and unburnt pulverized coal exist in the lower part of the coke bed, which may significantly affect the slag wettability. In an extreme condition, a non-wetting slag is more likely to block gas passage among coke particles from the upper side in the lower region of a BF. In this regard, both significant slag redistribution and local flooding may occur.

### B. Liquid Slag Flow Among the Spherical Particles

Compared with the slag flow in a funnel, a more realistic condition can be considered, such as a bed with spherical particles in a close-packed structure. As slag flows through the interstitial (void) space between spherical particles, it may partially or fully occupy this void space, depending on its properties and flow condition. To characterize the effect of this void space on the slag flow, particularly considering the narrowest part (neck) of the space, an equivalent diameter was used to represent the void area between three touching particles on a horizontal plane across the centres of these particles. Note that the equivalent diameter was defined as the diameter of a circle with the same area as the void area between particles on the neck plane. Corresponding to a particle diameter of 10 mm similar to that used in high-temperature packed bed experiments,[20] the calculated equivalent diameter between three spherical particles is ~ 2.3 mm. For a loose random packing, the average neck size between particles will be larger than this value. Hence, the numerical investigations were carried out over a range of equivalent diameters (2 to 8 mm).

To reduce the computational cost, only a two-dimensional condition was used in the simulation. Considering the realistic condition is three-dimensional, it is expected that two-dimensional modelling results are qualitative, but also constructive. Figure 10(a) shows the reduced geometry in a two-dimensional computational domain. As shown in Figure 10(a), the axis of symmetry between the two particles is used, so the labelled value (1 to 4 mm) corresponds to an actual neck size between two spherical particles varying from 2 to 8 mm. The initial condition for the slag flow was a slag column height between the particles of 2 mm commencing 1 mm above the neck (Figure 10(b)). The initial slag column heights are the same to permit the same initial liquid hydrostatic pressure for different scenarios. Using Slag C, a series of contact angles and neck sizes were applied to investigate their effects on the slag flow. For each neck diameter, a
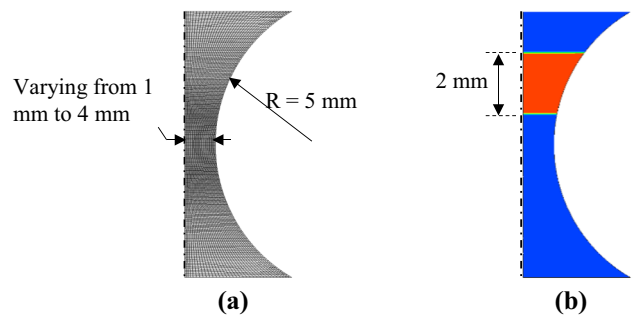


Fig. 10—(a) Dimensions of 2D computational domain and (b) initial slag condition. Note that R refers to the radius of the spherical particle.

range of slag wettability, from wetting to non-wetting conditions, was used, i.e. contact angle varying from 60 to 160 deg.

For each scenario, steady-state results at time $t = 0.3$ seconds were achieved and are given in Figures 11, 12, 13 and 14. It should be noted that in Figure 14(b), intermediate results are given because all slag in the space flowed out before 0.3 seconds. The contact area between slag and particle significantly changes as the neck diameter and contact angle increase. It is relatively easy for a slag with a high contact angle to pass through the gap between particles with a large neck diameter. As the contact angle increases within a certain range (Figures 11(a), 12(a) and 13(a)), the contact area between the slag and particle surface decreases. For the cases with remaining slag in the gap between particles, the slag level becomes lower as the contact angle or neck diameter increases. As one or the other increase, the influence of the adhesive (capillary) force on the central part of the slag becomes less significant.

Generally, if the blockage does not occur, with increasing contact angle, the slag is likely to more easily pass through the gap between the particles. However, for a narrow neck size, a strong non-wetting slag can cause slag to be held up above the neck as shown in Figure 14(a), i.e. as the contact angle increases above a certain value (e.g. 160 deg in this case).

For a non-wetting liquid slag, with a relatively high ratio of attractive forces within the liquid to those between liquid and solid surface, i.e. a high ratio of cohesive force to adhesive force,[50] the liquid separates from the surface of the particles quite easily as it flows downwards and a more spherical droplet is formed. For a wetting liquid slag, the liquid is more likely to flow along the surface of particles and form a shape to a large degree dictated by the topological structure of the particles. Therefore, on this basis, correlations predicting the amount of slag remaining or held up in a packed bed should reflect the following,

- for a contact angle of 90 deg, the static holdup is not zero,
- the potential zero static holdup at a contact angle of 180 deg is conditional and closely related to the packing condition and
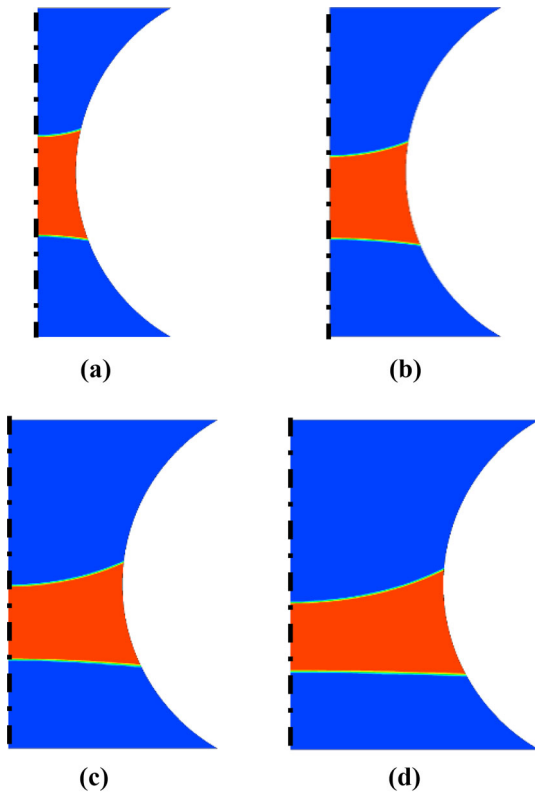
Fig. 11—Static holdup distribution for a contact angle of 60 deg and a neck diameter of (*a*) 2; (*b*) 4; (*c*) 6; and (*d*) 8 mm at time $t = 0.3$ s.
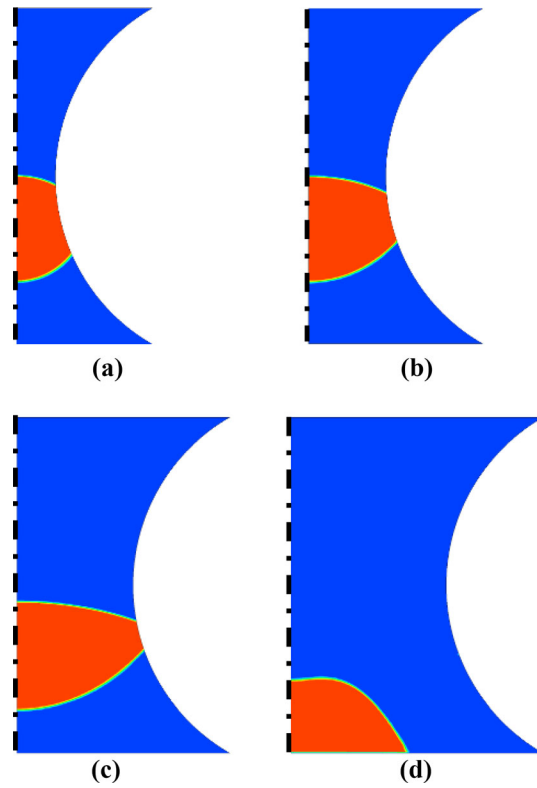


Fig. 13—Static holdup distribution for a contact angle of 120 deg and a neck diameter of (*a*) 2; (*b*) 4; (*c*) 6; (*d*) 8 mm at time $t = 0.3$ s.
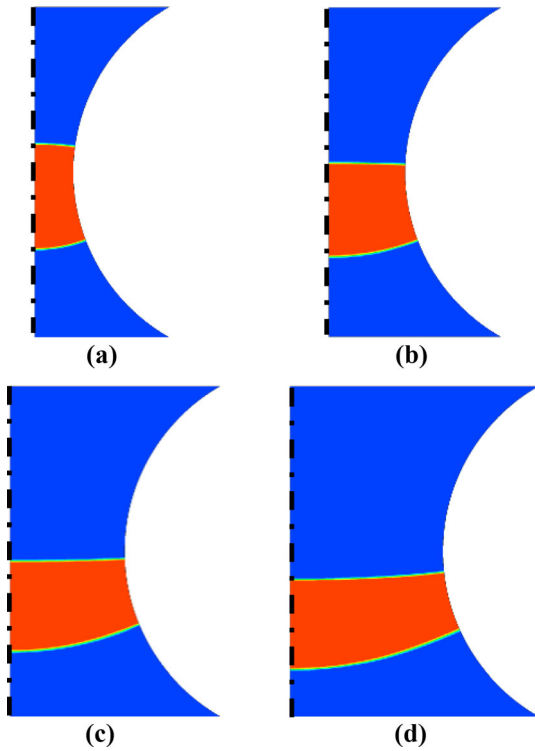


Fig. 12—Static holdup distribution for a contact angle of 90 deg and a neck diameter of (*a*) 2; (*b*) 4; (*c*) 6; and (*d*) 8 mm at time $t = 0.3$ s.
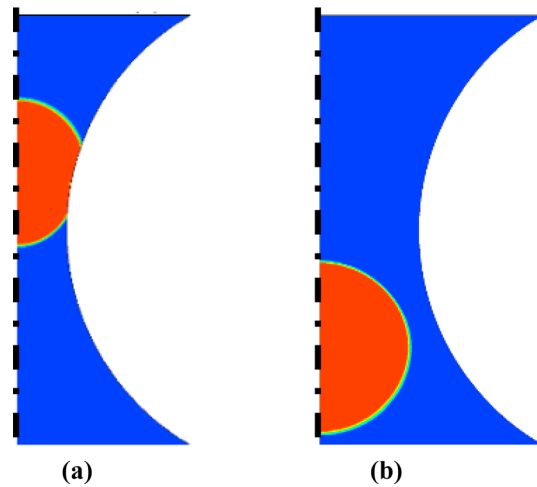


Fig. 14—Static holdup distribution for a contact angle of 160 deg and a neck diameter of (*a*) 2 and (*b*) 4 mm at time $t = 0.3$ s and 0.04 s, respectively.

- for a certain packing condition, an optimum contact angle may exist for a minimum static holdup.

While the actual BF lower zone system is more complex than the simplified systems evaluated in this investigation, the latter provides further understanding that helps clarify some of the flow features occurring in the former. For example, in relation to variations in slag wettability, the numerical results describing hanging and

blockage phenomena indicate that the residence time and the amount of slag remaining between the coke particles could significantly change in the various slag formation zones in the BF. This may, in turn, cause variations in coalescence and division of slag rivulets within the bed and/or impact the contact made between slag and liquid iron, coke particles and ascending gas in these zones. Another example is the effect of local packing structure, which must also be assessed in these zones. The numerical results indicate that although a non-wetting condition can generally help improve the slag flow, a poorer condition such as a narrow neck size between particles can lead to blockage of slag. This suggests that a threshold exists with respect to packing structure, and beyond this, any consideration to adjust slag wettability for improved flow in the BF is expected to be limited. In this regard, the microscopic scale modelling undertaken in this research can potentially be extended to a larger scale for characterizing the interaction between phases for better BF process control and optimization.

## V. CONCLUSIONS

The molten slag flow through the inter-particle voids of a packed bed was numerically studied as part of an investigation of the molten liquid flow in the blast furnace lower zone. The slag interface and volume distribution were tracked at a particle scale based on the Volume of Fluid method. It was found that

- Changing slag wettability significantly affected the slag behaviour in a funnel. The status of the remaining slag in the funnel was differentiated in terms of the blockage in the upper part and hanging in the lower part of the funnel corresponding to different slag wettabilities.
- A critical funnel neck size, through which no slag flowed was experimentally established and confirmed by CFD modelling. The influence of slag wettability on the occurrence of blockage was also determined via numerical modelling.
- The flow behaviour of slag through the gap between the spherical particles in relation to the slag wettability demonstrates that for a certain packing condition, an optimum contact angle may exist that minimizes static holdup in a packed bed.

These findings highlight that this numerical approach is very helpful to understand the effect of slag properties on liquid flow, to provide guidance to evaluate empirical liquid holdup correlations generated at macroscopic scale, and to control slag properties in order to maintain and improve BF permeability and productivity.

In terms of better understanding and quantifying the complex phase interactions occurring in the lower part of the BF, further clarification of molten liquids flow will include:

- investigating the variation of slag wettability under more realistic conditions considering, for example, the existence of FeO and fines in the slag; and

- from a macroscopic perspective, quantifying the critical conditions for slag holdup using feasible and reliable correlations.

These developments will provide a foundation to study the interaction between liquid iron and slag under various BF operating conditions. Future research and outcomes in these areas will play a significant role in BF process control and optimization.

## REFERENCES

1. M. Naito, K. Takeda, and Y. Matsui: *ISIJ Int.*, 2015, vol. 55, pp. 7–35.
2. Y. Omori: *Blast Furnace Phenomena and Modelling*, Elsevier Applied Science, London, 1987.
3. T. Usui, H. Kawabata, Z.I. Morita, and K. Masamori: *ISIJ Int.*, 1993, vol. 33, pp. 687–96.
4. T. Sugiyama, T. Nakagawa, H. Sibaike, and Y. Oda: *Tetsu to Hagane*, 1987, vol. 73, pp. 2044–51.
5. J.F. Elliott, R.A. Buchanan, and J.B. Wagstaff: *J. Met.*, 1952, vol. 194, pp. 709–17.
6. J. Szekely and J. Mendrykowski: *Chem. Eng. Sci.*, 1972, vol. 27, pp. 959–63.
7. N. Standish and J.B. Drinkwater: *J. Met.*, 1972, vol. 24, pp. 43–45.
8. T. Fukutake and V. Rajakumar: *Trans. Iron Steel Inst. Jpn*, 1982, vol. 22, pp. 355–64.
9. T.S. Pham, D. Pinson, A.B. Yu, and P. Zulli: *Chem. Eng. Sci.*, 1999, vol. 54, pp. 5339–45.
10. G.S. Gupta, J.D. Litster, V.R. Rudolph, E.T. White, and A. Domanti: *ISIJ Int.*, 1996, vol. 36, pp. 32–39.
11. S.J. Chew, G.X. Wang, A.B. Yu, and P. Zulli: *Ironmak. Steelmak.*, 1997, vol. 24, pp. 392–400.
12. H. Kawabata, K. Shinmyou, T. Harada, and T. Usui: *ISIJ Int.*, 2005, vol. 45, pp. 1474–81.
13. Y. Bando, S. Hayashi, A. Matsubara, and M. Nakamura: *ISIJ Int.*, 2005, vol. 45, pp. 1461–65.
14. H. Ohgusu, Y. Sassa, Y. Tomita, K. Tanaka, and M. Hasegawa: *Tetsu to Hagane*, 1992, vol. 78, pp. 1164–70.
15. W.M. Husslage, M.A. Reuter, R.H. Heerema, T. Bakker, and A.G.S. Steeghs: *Metall. Mater. Trans. B*, 2005, vol. 36B, pp. 765–76.
16. I.H. Jeong, H.S. Kim, and Y. Sasaki: *ISIJ Int.*, 2013, vol. 53, pp. 2090–98.
17. D. Jang, M. Shin, J.S. Oh, H.S. Kim, S.H. Yi, and J. Lee: *ISIJ Int.*, 2014, vol. 54, pp. 1251–55.
18. H.L. George, B.J. Monaghan, R.J. Longbottom, S.J. Chew, and P.R. Austin: *ISIJ Int.*, 2013, vol. 53, pp. 1172–79.
19. H.L. George, R.J. Longbottom, S.J. Chew, D.J. Pinson, and B.J. Monaghan: *ISIJ Int.*, 2014, vol. 54, pp. 1790–96.
20. H.L. George, R.J. Longbottom, S.J. Chew, and B.J. Monaghan: *ISIJ Int.*, 2014, vol. 54, pp. 820–26.
21. J.S. Oh and J. Lee: *J. Mater. Sci.*, 2016, vol. 51, pp. 1813–19.

22. M. Hino, T. Nagasaka, A. Katsumata, K.-I. Higuchi, K. Yamaguchi, and N. Kon-No: *Metall. Mater. Trans. B*, 1999, vol. 30B, pp. 671–83.
23. T. Sugiyama and M. Sugata, *Nippon Steel Technical Report* 1987, pp. 32–42.
24. J. Szekely and Y. Kajiwara: *Trans. Iron Steel Inst. Jpn.*, 1979, vol. 19, pp. 76–84.
25. Y. Ohno and M. Schneider: *Tetsu to Hagane*, 1988, vol. 74, pp. 1923–30.
26. J. Wang, R. Takahashi, and J. Yagi: *Tetsu to Hagane*, 1991, vol. 77, pp. 1585–92.
27. Y. Eto, K. Takeda, S. Miyagawa, H. Itaya, and S. Taguchi: *ISIJ Int.*, 1994, vol. 33, pp. 681–86.
28. G.X. Wang, S.J. Chew, A.B. Yu, and P. Zulli: *Metall. Mater. Trans. B*, 1997, vol. 28B, pp. 333–43.
29. G.X. Wang, S.J. Chew, A.B. Yu, and P. Zulli: *ISIJ Int.*, 1997, vol. 37, pp. 573–82.
30. S.J. Chew, P. Zulli, and A. Yu: *ISIJ Int.*, 2001, vol. 41, pp. 1112–21.
31. I.H. Jeong and S.M. Jung: *ISIJ Int.*, 2016, vol. 56, pp. 537–45.
32. T. Kon, S. Natsui, S. Ueda, R. Inoue, and T. Ariyama: *ISIJ Int.*, 2012, vol. 52, pp. 1565–73.
33. T. Kon, S. Natsui, S. Ueda, R. Inoue, and T. Ariyama: *ISIJ Int.*, 2013, vol. 53, pp. 590–97.
34. T. Kon, S. Natsui, S. Ueda, and H. Nogami: *ISIJ Int.*, 2015, vol. 55, pp. 1284–90.
35. S. Natsui, T. Kikuchi, R.O. Suzuki, T. Kon, S. Ueda, and H. Nogami: *ISIJ Int.*, 2015, vol. 55, pp. 1259–66.
36. S. Natsui, K.I. Ohno, S. Sukenaga, T. Kikuchi, and R.O. Suzuki: *ISIJ Int.*, 2018, vol. 58, pp. 282–91.
37. S. Natsui, K. Tonya, H. Nogami, T. Kikuchi, R.O. Suzuki, K.I. Ohno, S. Sukenaga, T. Kon, S. Ishihara, and S. Ueda: *Processes*, 2020, vol. 8, p. 221.
38. S. Natsui, A. Sawada, H. Nogami, T. Kikuchi, and R.O. Suzuki: *ISIJ Int.*, 2020, vol. 60, pp. 1445–52.
39. S. Natsui, A. Sawada, H. Nogami, T. Kikuchi, and R.O. Suzuki: *ISIJ Int.*, 2020, vol. 60, pp. 1453–60.
40. C.W. Hirt and B.D. Nichols: *J. Comput. Phys.*, 1981, vol. 39, pp. 201–25.
41. D.L. Youngs, In *Numerical Methods for Fluid Dynamics*, K.W. Morton and M.J. Baines, eds., Academic Press, New York, 1982.
42. J.U. Brackbill, D.B. Kothe, and C. Zemach: *J. Comput. Phys.*, 1992, vol. 100, pp. 335–54.
43. ANSYS Inc., ANSYS Fluent-19.1-User Online Manual, 2018.
44. D.G. Holmes and S.D. Connell, *9th Computational Fluid Dynamics Conference*, Buffalo, NY, USA, 1989.
45. J.P. Van Doormaal and G.D. Raithby: *Numer. Heat Transf.*, 1984, vol. 7, pp. 147–63.
46. K.C. Mills: *Slags Model (ed 1.07)*. National Physical Laboratory, UK, 1991.
47. P.V. Riboud, Y. Roux, L.D. Lucas, and H. Gaye: *Fachberichte Huttenpraxis Metallweiterverarbeitung*, 1981, vol. 19, pp. 859–69.
48. R.H. Perry and D.W. Green: *Perry's Chemical Engineering's Handbook*, 7th ed., McGraw-Hill, New York, 1997.
49. M. Hayashi, S. Sukenaga, K.I. Ohno, S. Ueda, K. Sunahara, and N. Saito: *Tetsu-To-Hagane*, 2014, vol. 100, pp. 211–26.
50. L.D. Landau and E.M. Lifshitz: *Fluid Mechanics*, Pergamon Press, New York, 1987.